NASA TM X-756

TECHNICAL MEMORANDUM

X-756

INVESTIGATION OF THE LOW-SUBSONIC AERODYNAMIC CHARACTERISTICS OF A MODEL OF A MODIFIED LENTICULAR REENTRY CONFIGURATION

By George M. Ware

Langley Research Center
Langley Station, Hampton, Va.

[redacted]

[redacted]

NATIONAL AERONAUTICS AND SPACE ADMINISTRATION
WASHINGTON
December 1962

[redacted]

NATIONAL AERONAUTICS AND SPACE ADMINISTRATION

TECHNICAL MEMORANDUM X-756

INVESTIGATION OF THE LOW-SUBSONIC AERODYNAMIC CHARACTERISTICS OF A MODEL OF A MODIFIED LENTICULAR REENTRY CONFIGURATION*

By George M. Ware

SUMMARY

An investigation has been made of the static stability and control characteristics at low-subsonic speeds of a modified lenticular reentry configuration. The model was nearly circular in planform with a large-radius lower surface and a highly cambered upper surface. The model was also equipped with two pylon-mounted fins.

The basic configuration (configuration 1) was longitudinally unstable about the design center of gravity, had a large negative pitching moment at zero angle of attack, and had a maximum lift-drag ratio of only 2.5. These adverse characteristics were mainly a result of disturbed or separated flow caused by fin-body interference. Modifying the fins and setting them at negative incidence (configuration 2) and adding a pylon-body fairing made the model longitudinally stable, produced a positive pitching moment at zero angle of attack, and almost doubled the lift-drag ratio. Configuration 2 with the pylon-body fairing was directionally unstable at an angle of attack of approximately 15°. Addition of a center-mounted vertical tail made the model stable over the angle-of-attack range. Differential deflection of the elevons as a roll control produced rather low rolling moments over the angle-of-attack range. Differential deflection of the "rudder-vons" as a yaw control produced adequate yawing moments but produced extremely large adverse rolling moments.

INTRODUCTION

An investigation is being conducted by the National Aeronautics and Space Administration to provide information on the aerodynamic characteristics of lifting-body configurations designed for controlled reentry into the earth's atmosphere (see refs. 1 to 6). The lifting-body type of reentry configuration is of considerable interest because it provides high usable volume for a given planform area, exposure to lower peak-heating rates than those of the ballistic type, and the controlled glide and landing capabilities of the winged configuration. The characteristics of one such lifting-body proposal, a lenticular configuration, are presented in references 7 to 13. The purpose of the present investigation is

*Title, Unclassified.

to provide aerodynamic information on a lenticular reentry configuration modified to give a volume distribution suitable to the placement of equipment and/or personnel. The model was nearly circular in planform with a large-radius lower surface and a highly cambered upper surface. The model was equipped with fins which fold up and are shielded by the body during the high-drag, high angle-of-attack reentry phase and then fold out to a 45° dihedral angle to provide static longitudinal and lateral stability during the glide landing.

The investigation consisted of force tests at angles of attack up to 45° to determine the static longitudinal and lateral stability and control characteristics of two configurations of the model.

SYMBOLS

The lateral data are referred to the body system of axes (fig. 1) and the longitudinal data are referred to the wind axes. All coefficients are based on a reference area of 11.7 square feet and a reference chord and span of 3.6 feet. The moments are referred to a point 2.6 feet aft of the nose of the model which corresponds to 51.8 percent of the reference chord.

b	reference span, ft
c	reference chord, ft
C_D	drag coefficient, D/qS
C_l	rolling-moment coefficient, M_X/qSb
ΔC_l	incremental rolling-moment coefficient
$C_{l_\beta} = \frac{\partial C_l}{\partial \beta}$	per degree
C_L	lift coefficient, L/qS
C_m	pitching-moment coefficient, M_Y/qSc
$C_{m,o}$	pitching moment at $\alpha = 0^\circ$
C_n	yawing-moment coefficient, M_Z/qSb
ΔC_n	incremental yawing-moment coefficient
$C_{n_\beta} = \frac{\partial C_n}{\partial \beta}$	per degree
C_Y	side-force coefficient, F_Y/qS

ΔC_Y	incremental side-force coefficient
$C_{Y_\beta} = \frac{\partial C_Y}{\partial \beta}$	per degree
D	drag, lb
F_Y	side force, lb
i	fin incidence, deg
L	lift, lb
L/D	lift-drag ratio
M_X	rolling moment, ft-lb
M_Y	pitching moment, ft-lb
M_Z	yawing moment, ft-lb
q	dynamic pressure, $\rho V^2/2$, lb/sq ft
r	radius, in.
S	planform area, sq ft
V	free-stream velocity, ft/sec
X,Y,Z	reference axes unless otherwise noted
α	angle of attack, deg
β	angle of sideslip, deg
Γ	fin dihedral angle (measured from the horizontal), deg
δ_a	aileron deflections, $\delta_{e,R} - \delta_{e,L}$, deg
δ_e	elevator deflection (positive when trailing edge down), deg
$\delta_{e,L}$	left elevon deflection (positive when trailing edge down), deg
$\delta_{e,R}$	right elevon deflection (positive when trailing edge down), deg
$\delta_{r,L}$	left ruddervon deflection (positive trailing edge left), deg
$\delta_{r,R}$	right ruddervon deflection (positive trailing edge left), deg
ρ	air density, slugs/cu ft

APPARATUS AND MODEL

The model was tested in a low-speed tunnel with a 12-foot octagonal test section at the Langley Research Center. The model was also tested in the Langley full-scale tunnel, which has a 30- by 60-foot open-throat test section, to determine blockage corrections to apply to the data from the smaller tunnel and to determine Reynolds number effects. The same sting-support system and an internally mounted six-component strain-gage balance were used for the tests in both tunnels. No base-pressure corrections were applied to the data.

A three-view drawing of configuration 1 is presented in figure 2(a). The model was equipped with two pylon-mounted fins with hinge lines parallel to the longitudinal body reference line. These fins could be rotated and set at any dihedral angle from 0° to 90°, with the normal or design position for gliding flight being at 45°. The fins were equipped with ruddervons which were to be used for yaw and pitch control. The model also had elevons mounted on the body for pitch and roll control.

Early in the test program it became desirable to test configuration 1 with other fin arrangements. Since it was difficult to change the position of the original fins, a set of flat-plate fins was constructed. The fins and their mounting positions are shown in figure 2(b). The flat-plate fins were set at a dihedral angle of 45° and could be positioned at various hinge-line incidence settings and at various lateral positions on the pylon.

A three-view drawing of configuration 2 is shown in figure 3. Configuration 2 was made by modifying the fin pylons of configuration 1 by moving them farther outboard and inclining the upper surfaces to produce a fin incidence of -18°. The fins were also revised to a symmetrical cross section. Other modifications which were tested are shown in figure 3 and include a pylon-body fairing and a vertical tail mounted in the center of the upper surface of the body.

Photographs of configuration 1 and configuration 2 with the pylon-body fairing are presented in figure 4.

TESTS

Force tests were made over an angle-of-attack range from -2° to 45° to determine the effect of fin position and incidence and the effect of Reynolds number on the static longitudinal stability characteristics of configuration 1. Both the longitudinal and lateral stability and control characteristics of configuration 2 were investigated. The lateral stability tests were conducted at angles of sideslip of 5° and -5° at various angles of attack from 0° to 45°. Also investigated were the effects of fins, fin dihedral angle, pylon-body fairing, and vertical tail on the stability characteristics of the model.

The Reynolds number investigation was conducted in the Langley full-scale tunnel at Reynolds numbers of 3.15, 2.11, and 1.21 times 10^6 based on the model

reference chord of 3.6 feet. The remaining tests were made in the 12-foot low-speed tunnel at a dynamic pressure of 4.0 pounds per square foot and a speed of 58 feet per second and a Reynolds number of 1.33×10^6.

RESULTS AND DISCUSSION

Longitudinal Characteristics

Preliminary force tests made in the Langley full-scale tunnel indicated that increasing the Reynolds number from 1.21×10^6 to 3.15×10^6 had no large effects on the characteristics of the model and that the data from tests conducted in the 12-foot low-speed tunnel, which were made only at a Reynolds number 1.33×10^6, should be representative of results obtained at somewhat higher Reynolds numbers.

Configuration 1.- The longitudinal characteristics of configuration 1 are presented in figure 5. The data show that the body alone, body and elevons, and the complete model were all highly unstable over most of the angle-of-attack range and had large negative values of $C_{m,o}$. These characteristics would make it virtually impossible to achieve a usable longitudinally stable condition by shifting the center of gravity forward because of the very large out-of-trim moments that would be encountered. The addition of the elevons and the fins greatly increased the lift coefficient at the higher angles of attack. The maximum L/D value of 2.5 for the complete model was only about half as great as that for the body alone or for the body with elevons.

Tuft studies indicated that the low L/D value for the complete model was a result of disturbed flow or flow separation caused by mutual interference effects between the body and the fins. At an angle of attack of 0°, the flow was observed to be very disturbed in the region between the fin hinge line and the body. As the angle of attack was increased, the region of separated flow moved toward the tip of the fin and spread over the upper rear portion of the body.

In an effort to determine a better arrangement for the fins, exploratory tests were made with relatively thin flat-plate fins to facilitate fin-position changes. In these tests, the fins were mounted on the upper surfaces of the pylons so that they were alined with the outside or inside edge of the pylon or were mounted on the outside surfaces of the pylons, with $i = 0^\circ$ and $\Gamma = 45^\circ$ for all configurations. (See fig. 2(b).) The data obtained in these tests, together with data for the model with the original fins, are presented in figure 6. The characteristics of the model with the flat-plate fins in the inboard position were about the same as those of the model with the original fins. When the flat-plate fins were moved to the outboard or side positions, however, there was a large decrease in longitudinal instability and a large increase in lift coefficient, lift-curve slope, and L/D values up to an angle of attack of about 5° or 10° which indicated a change in the fin-body interference effects. In this angle-of-attack range, the flow over the fins apparently separated with a resulting loss in lift and an unstable break in the pitching-moment curve.

The effect of incidence of the flat-plate fins mounted on the outside surface of the pylons is presented in figure 7. These data show that increasing negative

fin incidence decreased the longitudinal instability of the model at moderate angles of attack, added positive increments of pitching moment over the angle-of-attack range, and decreased lift at low angles of attack. These effects of fin incidence came from a change in the effective angle of attack of the fins which resulted in different fin lift and stall angle with respect to the angle of attack of the model. The maximum L/D value for the configuration was therefore reduced with increasing fin incidence, and the point of the maximum L/D value was shifted to a higher angle of attack.

From the results of these tests, it appears that the general characteristics of the model could be greatly improved by redesigning the fins. With the information gathered from the exploratory tests, the model was therefore modified by changing the spanwise location, incidence, and cross section of the fin (see fig. 3); the modified model was designated configuration 2.

Configuration 2.- The longitudinal characteristics of configuration 2 are compared in figure 8 with those of the basic model (configuration 1). These data show that the fin incidence incorporated in configuration 2 produced a positive $C_{m,o}$, and in general, the model had a more linear variation of lift and pitching moment with angle of attack. While these improvements were significant, the L/D values for the model with fins on were not as high as those for the model with the fins off, and the variation of pitching moment with angle of attack was still unsatisfactory.

Tuft studies were again made and showed that while the flow characteristics between the fin and the body were better for configuration 2 than for configuration 1, the flow was still disturbed in this region. In an effort to smooth the flow, the model was fitted with a fairing that extended horizontally between the top of the pylon and the body (see fig. 3). The effect of the fairing is presented in figure 9 for configuration 2 with fins on and off. The data show that the use of the fairing increased the stability of the complete model, increased the lift-curve slope up to an angle of attack of 16°, and increased the maximum L/D value. In this case, the maximum L/D value for the complete model was slightly greater and occurred at a higher angle of attack than for the fins-off condition. An abrupt break in the lift curve and an unstable break in the pitching-moment curve occurred at an angle of attack of about 13°, apparently because of fin stall. With fins off, the fairing caused a small reduction in longitudinal stability, reduction in lift at the higher angles of attack, and a large reduction in L/D values.

Although the longitudinal characteristics of configuration 2 with the pylon-body fairing are appreciably better than those of configuration 1, it should be pointed out that this is not considered to be an optimum configuration. A more detailed development study, which was beyond the scope of this investigation, would probably result in further improvement in the characteristics of this type of vehicle.

It should also be mentioned that configurations of this general type have been shown in reference 12 to lose longitudinal stability at high-subsonic speeds. Although no tests were made at these speeds in the present investigation, a possible means of compensating for any decrease in longitudinal stability is shown

in figure 10 where fin dihedral angle is varied for configuration 2 with the pylon-body fairing on. As might be expected, the stability of the model was increased as the fins approached the horizontal, and the lift of the model was also increased at the higher angles of attack. Fin dihedral angle had only a relatively small effect on the L/D values. The difference between the maximum L/D value for $\Gamma = 45^\circ$ in figure 10 and in previous figures is probably the result of slight differences in pylon-body fairing which was removed at various times during the test program and then rebuilt.

The effect of ruddervon and elevon deflection as a pitch control is presented in figures 11 and 12, respectively. The ruddervon tests were made without and with the pylon-body fairing. These data (figs. 11(a) and 11(b)) show that ruddervon deflection produced approximately the same incremental pitching moment at low angles of attack with the fairing on or off. At the higher angles of attack, as the flow over the fins became disturbed and separated, the ruddervons lost much of their effectiveness. Ruddervon deflection also had a pronounced effect on the L/D value. Downward ruddervon deflection increased the maximum L/D value, whereas upward deflection resulted in a rather large decrease in the L/D value.

The elevon-control data presented in figure 12 were only obtained with fairing off and show that the elevons were relatively ineffective at low angles of attack but increased in effectiveness above the fin stall angle. This trend is opposite to that of the ruddervons. Elevon deflection produced only a small change in the maximum L/D value.

Lateral Characteristics

The lateral stability data, which were obtained only for configuration 2, are presented in the form of the variation of the stability derivatives C_{Y_β}, C_{n_β}, and C_{l_β} with angle of attack. The values of the derivatives were obtained by taking the difference between the values of the coefficients measured at sideslip angles of 5° and -5°. Inasmuch as the tests were only made at sideslip angles of $\pm 5^\circ$, the derivative data should be used only to provide approximate comparisons of the various configurations and to indicate trends.

The lateral stability characteristics of configuration 2 with fins off and on, with pylon-body fairing, and with a center-mounted vertical tail are presented in figure 13. The body alone was directionally unstable up to about an angle of attack of 14° but became increasingly stable above this angle of attack. The addition of fins provided an increment of stability at low angles of attack, and the model was stable up to about an angle of attack of 7°. The fins were destabilizing over the remainder of the angle-of-attack range but the model was stable above an angle of attack of 15° because of the stabilizing contribution of the body. The loss of fin effectiveness is believed to be associated with the previously discussed fin-body interference which caused premature fin stall. The addition of the fairing reduced the degree of instability that the model experienced as well as the unstable angle-of-attack range. Addition of a center-mounted vertical tail produced an approximately constant increment of positive stability, and the model was stable over the angle-of-attack range. The effective-dihedral

parameter $-C_{l_\beta}$ was also greatly affected by the addition of the various components. The fins produced a large increment in $-C_{l_\beta}$ at low angles of attack, but a sharp break occurred at an angle of attack of 5° which corresponded to the break in the C_{n_β} curve. The fairing allowed the effective-dihedral parameter to increase up to about an angle of attack of 15° before falling off sharply. The addition of the vertical tail had little effect except to increase the parameter at the higher angles of attack.

The effect of fin dihedral angle on the lateral stability characteristics of the model is presented in figure 14. These data show that rotating the fins from $\Gamma = 30°$ to 60° increased the directional stability at the lower angles of attack but had relatively little effect on the stability of the model at the higher angles of attack. Even at a fin dihedral angle of 60°, the model had a region of directional instability around an angle of attack of 15°. The trend of the effective-dihedral parameter was unchanged by increasing fin dihedral, but the magnitude of the parameter was increased at the lower angles of attack.

The lateral control characteristics of the elevons and ruddervons are presented in figure 15. The data show that differential deflection of the elevons as a roll control produced rather low rolling moments over the angle-of-attack range and small adverse yawing moments. Differential deflection of the ruddervons, which are intended to be used primarily as a yaw control, produced yawing moments that decreased with increasing angle of attack, but the ruddervons also produced extremely large values of adverse rolling moments. These data indicate that the elevons would probably be inadequate as a roll control and that the ruddervons could provide a powerful roll control but would introduce large adverse yawing moments. It appears that the use of a center-mounted vertical tail could provide one solution to the lateral control problem as well as to increase the directional stability of the model. With this configuration, a rudder would be used as the yaw control and should be powerful enough to balance out the adverse yaw of the ruddervons which would then make possible the use of the ruddervons as a roll control.

SUMMARY OF RESULTS

The results of the investigation to determine the low-subsonic aerodynamic characteristics of a model of a modified lenticular reentry configuration may be summarized as follows:

1. The basic configuration (configuration 1) was longitudinally unstable, had a large negative pitching moment at zero angle of attack, and had a maximum lift-drag value of only 2.5. These adverse characteristics were a result of disturbed or separated flow caused by fin-body interference.

2. Modifying the fins and setting them at negative incidence (configuration 2) and adding a pylon-body fairing made the model longitudinally stable, produced a positive pitching moment at zero angle of attack, and almost doubled the maximum lift-drag value.

3. Configuration 2 with the pylon-body fairing was directionally unstable around an angle of attack of 15°. Addition of a center-mounted vertical tail made the model stable over the angle-of-attack range.

4. Differential deflection of the elevons as a roll control produced rather low rolling moments over the angle-of-attack range. Differential deflection of the ruddervons as a yaw control produced adequate yawing moments but produced extremely large adverse rolling moments.

Langley Research Center,
National Aeronautics and Space Administration,
Langley Station, Hampton, Va., August 15, 1962.

REFERENCES

1. Eggers, Alfred J., Jr., and Wong, Thomas J.: Re-entry and Recovery of Near-Earth Satellites, With Particular Attention to a Manned Vehicle. NASA MEMO 10-2-58A, 1958.

2. Savage, Howard F., and Tinling, Bruce E.: Subsonic Aerodynamic Characteristics of Several Blunt, Lifting, Atmospheric-Entry Shapes. NASA MEMO 12-24-58A, 1959.

3. Hassell, James L., Jr.: Investigation of the Low-Subsonic Stability and Control Characteristics of a 1/3-Scale Free-Flying Model of a Lifting-Body Reentry Configuration. NASA TM X-297, 1960.

4. Hassell, James L., Jr., and Ware, George M.: Investigation of the Low-Subsonic Stability and Control Characteristics of a 0.34-Scale Free-Flying Model of a Modified Half-Cone Reentry Vehicle. NASA TM X-665, 1962.

5. Dennis, David H., and Edwards, George G.: The Aerodynamic Characteristics of Some Lifting Bodies. NASA TM X-376, 1960.

6. Ware, George M.: Low-Subsonic-Speed Static Stability of Right-Triangular-Pyramid and Half-Cone Lifting Reentry Configurations. NASA TN D-646, 1961.

7. Ware, George M.: Static Stability and Control Characteristics at Low-Subsonic Speeds of a Lenticular Reentry Configuration. NASA TM X-431, 1960.

8. Mugler, John P., Jr., and Olstad, Walter B.: Static Longitudinal Aerodynamic Characteristics at Transonic Speeds of a Lenticular-Shaped Reentry Vehicle. NASA TM X-423, 1960.

9. Jackson, Charlie M., Jr., and Harris, Roy V., Jr.: Static Longitudinal Stability and Control Characteristics at a Mach Number of 1.99 of a Lenticular-Shaped Reentry Vehicle. NASA TN D-514, 1960.

10. Demele, Fred A., and Brownson, Jack J.: Subsonic Longitudinal Aerodynamic Characteristics of Disks With Elliptic Cross Sections and Thickness-Diameter Ratios From 0.225 to 0.425. NASA TN D-788, 1961.

11. Lazzeroni, Frank A.: Aerodynamic Characteristics of Two Disk Re-entry Configurations at a Mach Number of 2.2. NASA TM X-567, 1961.

12. Demele, Fred A., and Brownson, Jack J.: Subsonic Aerodynamic Characteristics of Disk Re-entry Configurations With Elliptic Cross Sections and Thickness-Diameter Ratios of 0.255 and 0.325. NASA TM X-566, 1961.

13. Lazzeroni, Frank A.: Experimental Investigation of a Disk-Shaped Reentry Configuration at Transonic and Low Supersonic Speeds. NASA TM X-652, 1962.

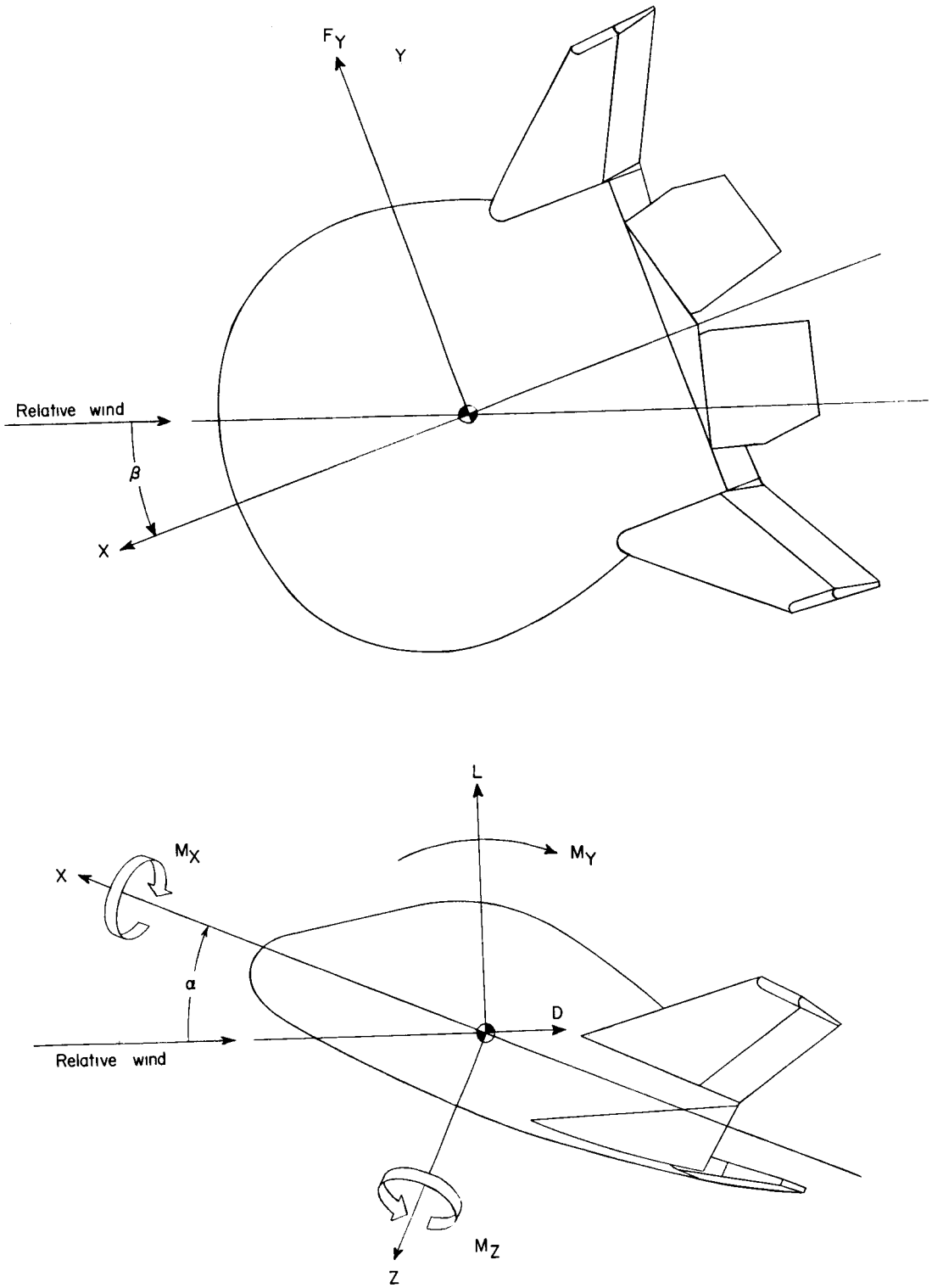

Figure 1.- Sketch of axis system used in investigation. Arrows indicate positive direction of forces, moments, and angles.

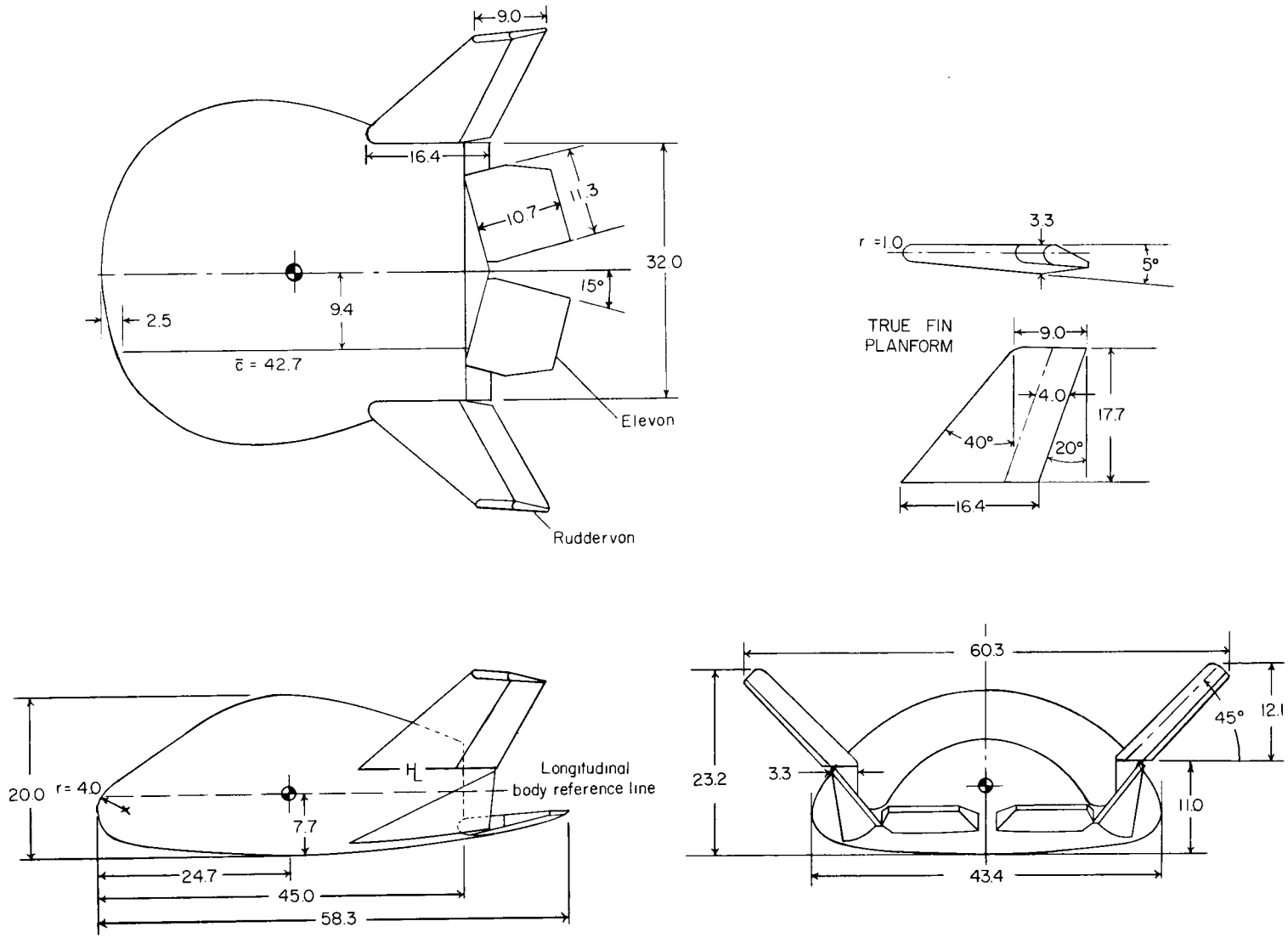

(a) Configuration 1.

Figure 2.- Three-view drawing of the basic model used in the investigation. All dimensions are in inches.

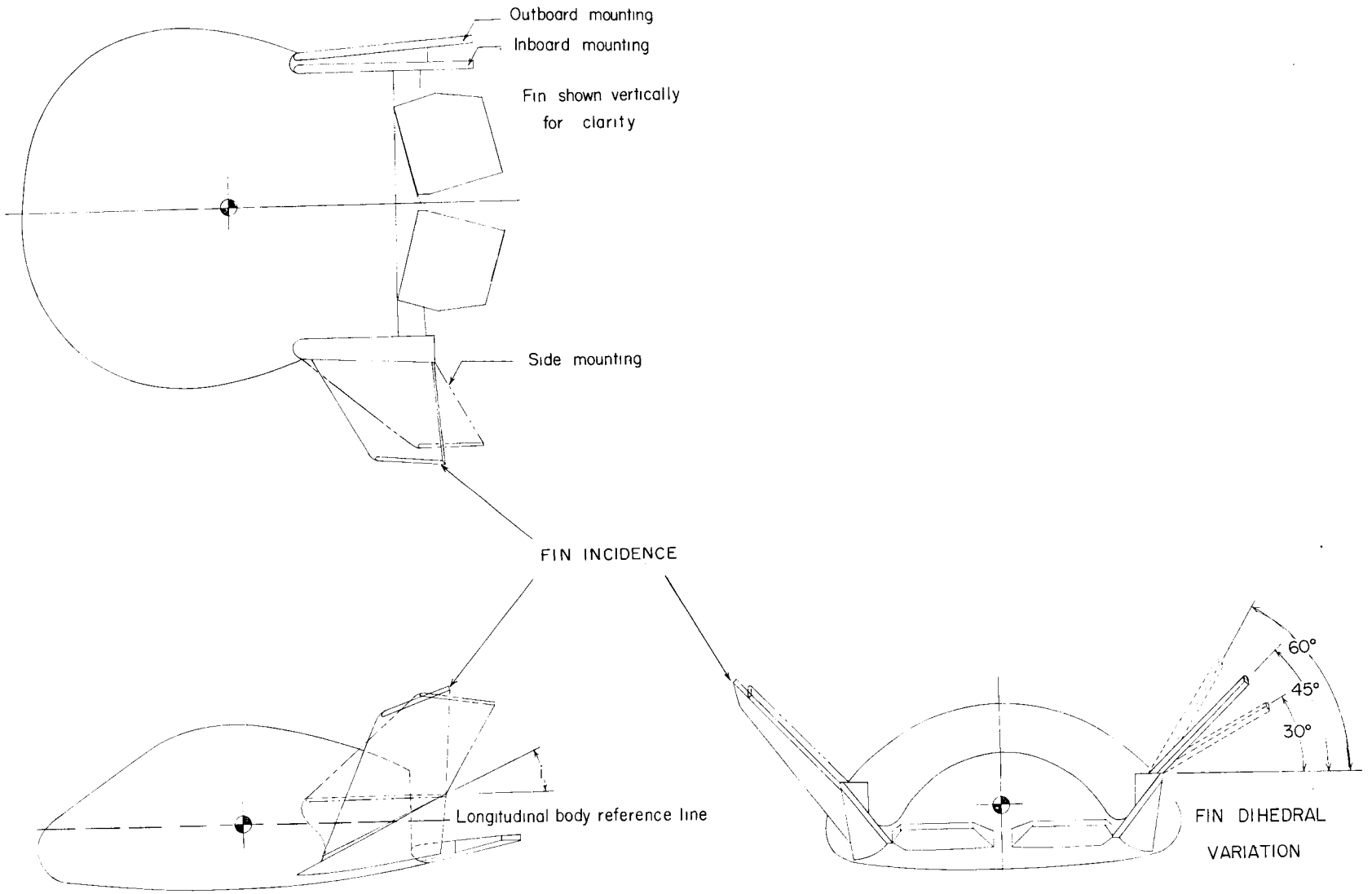

(b) Sketches of configuration 1 showing flat-plate fin arrangements.

Figure 2.- Concluded.

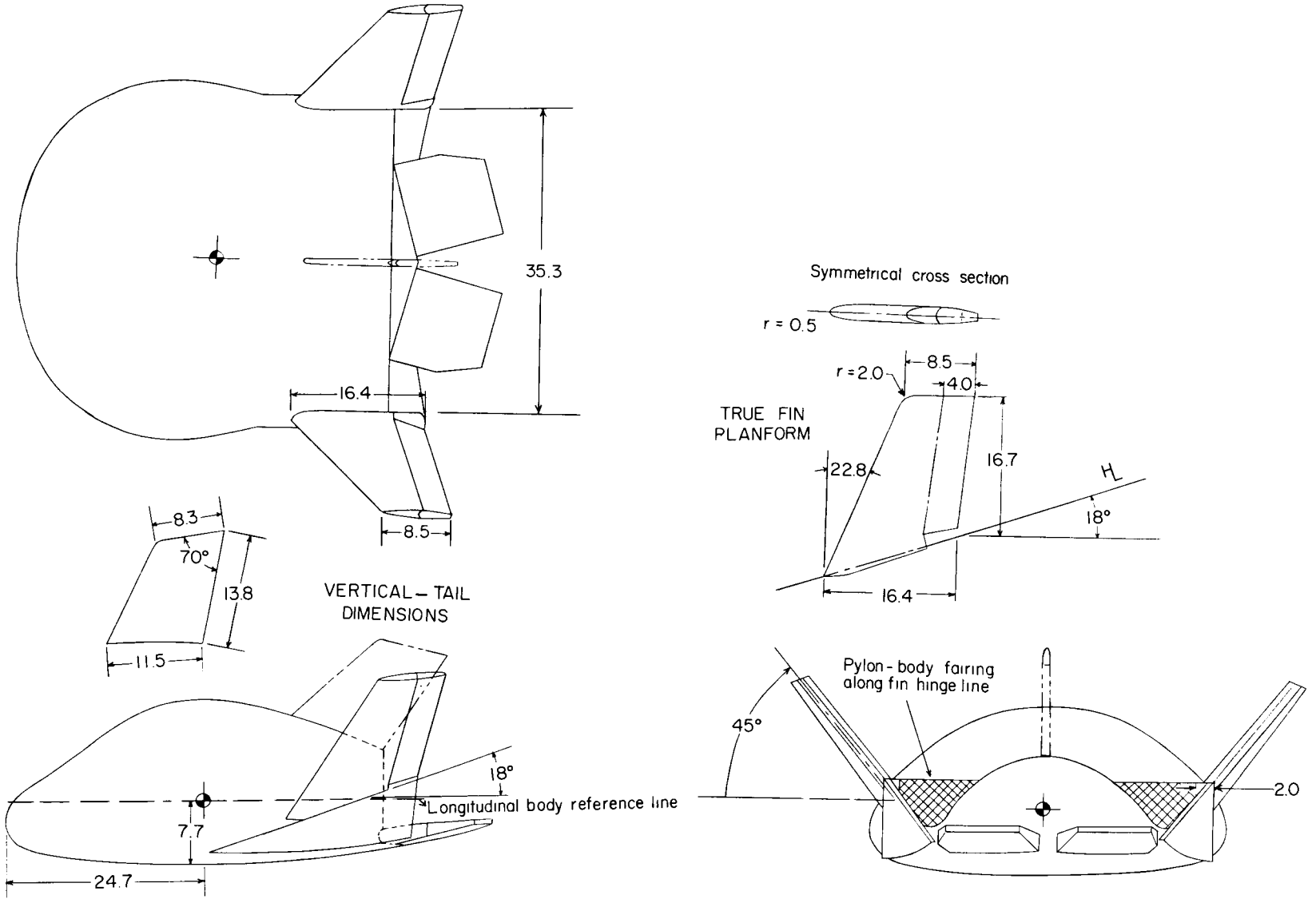

Figure 3.- Three-view drawing of configuration 2. All dimensions are in inches.

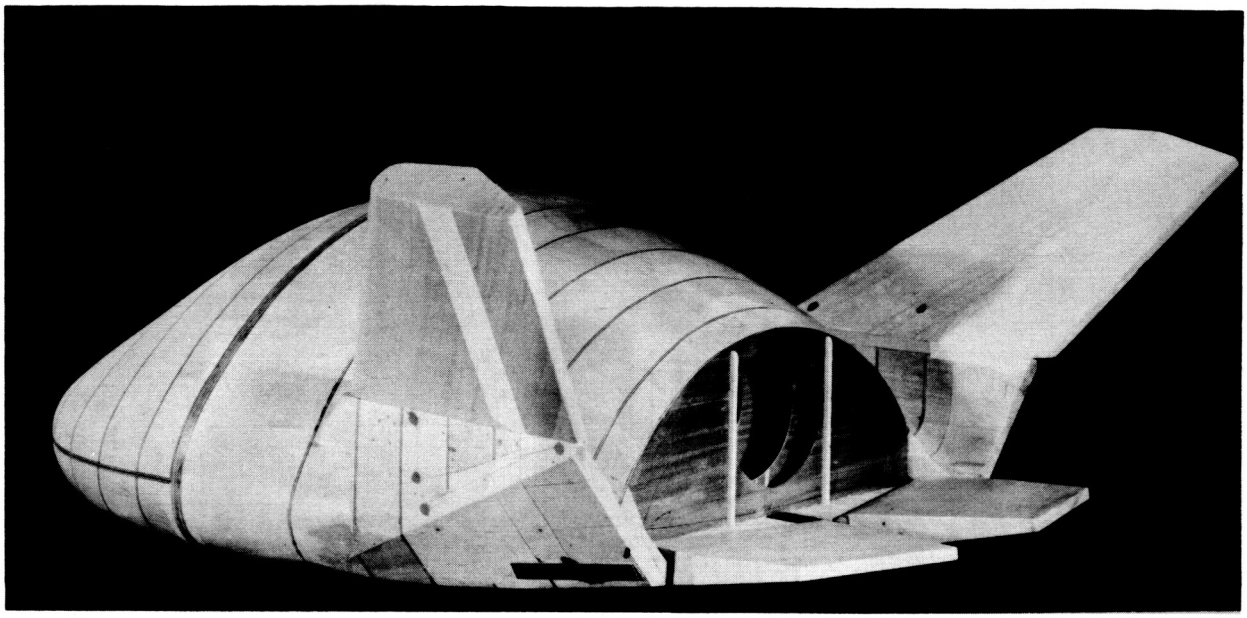

(a) Configuration 1. L-61-4442

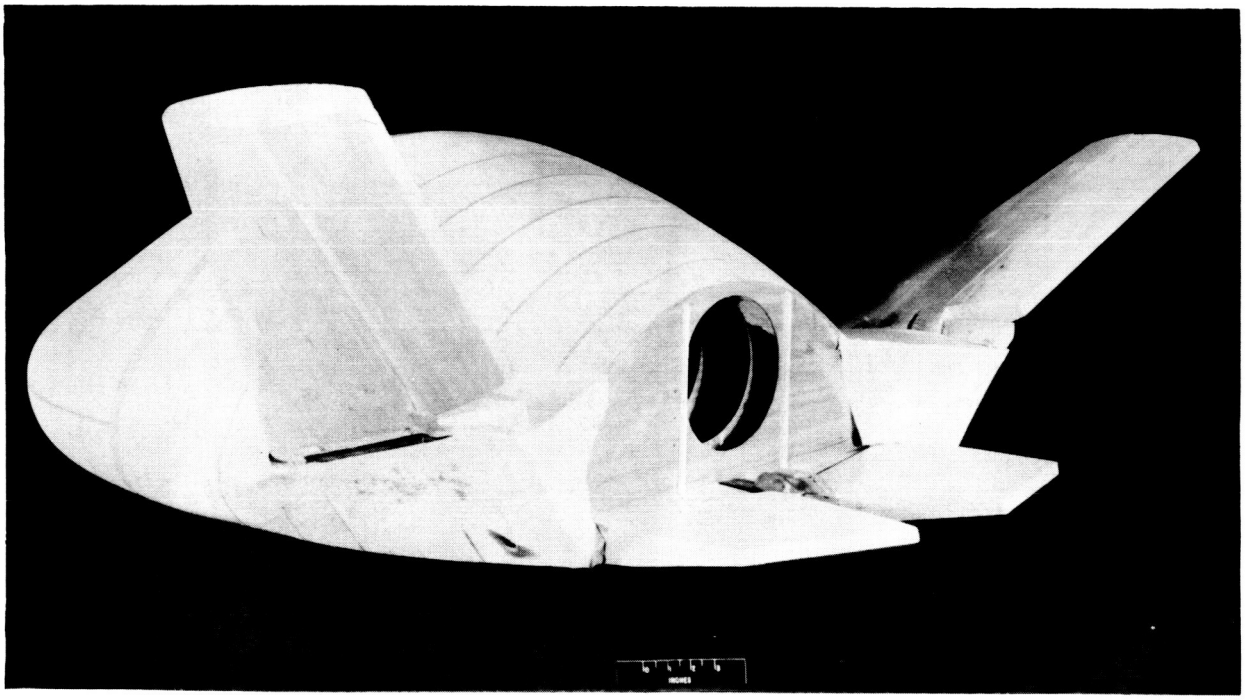

(b) Configuration 2 with pylon-body fairing. L-62-2455

Figure 4.- Photographs of models used in the investigation.

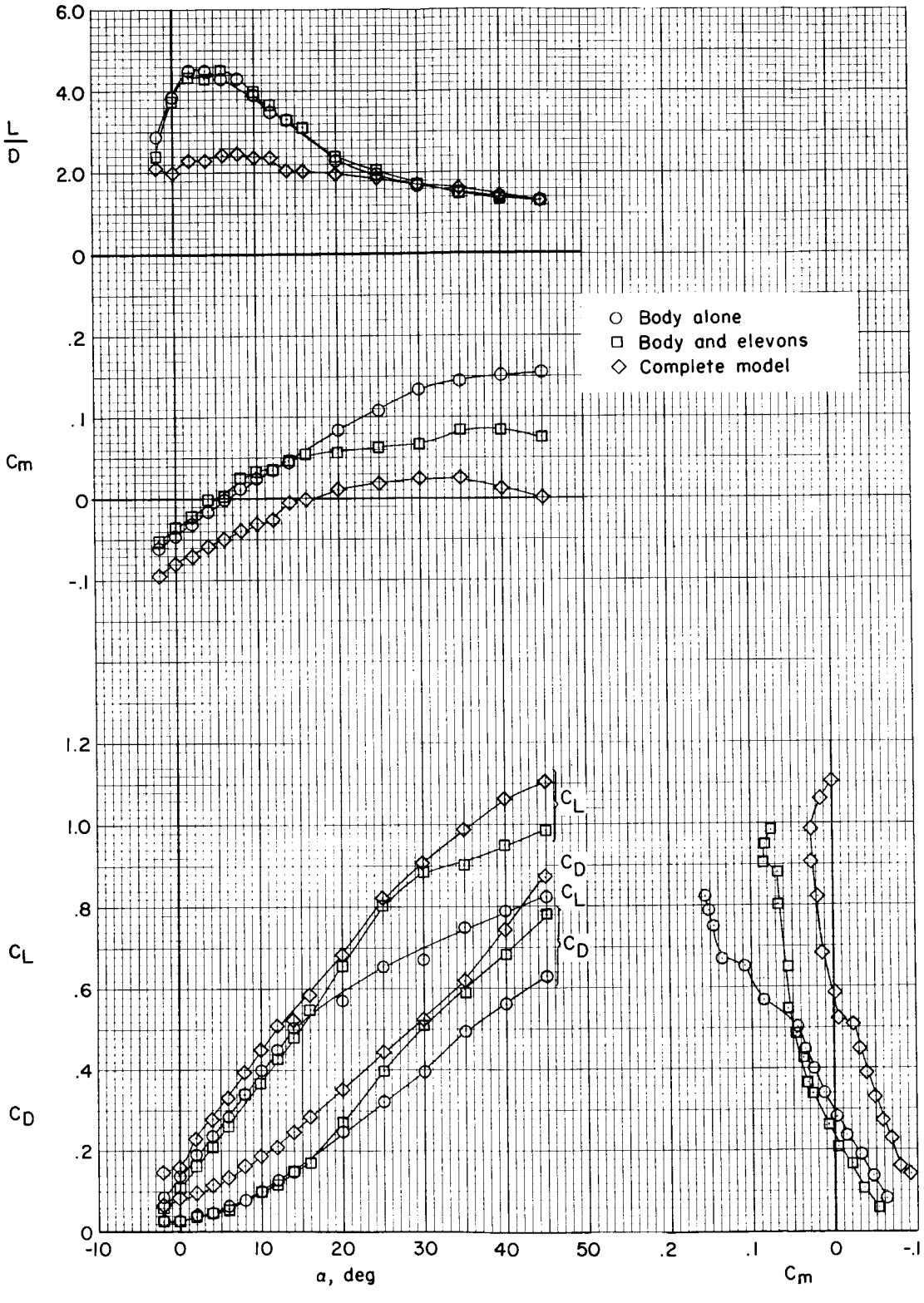

Figure 5.- Longitudinal stability characteristics of configuration 1. $\beta = 0^{\circ}$; $\Gamma = 45^{\circ}$.

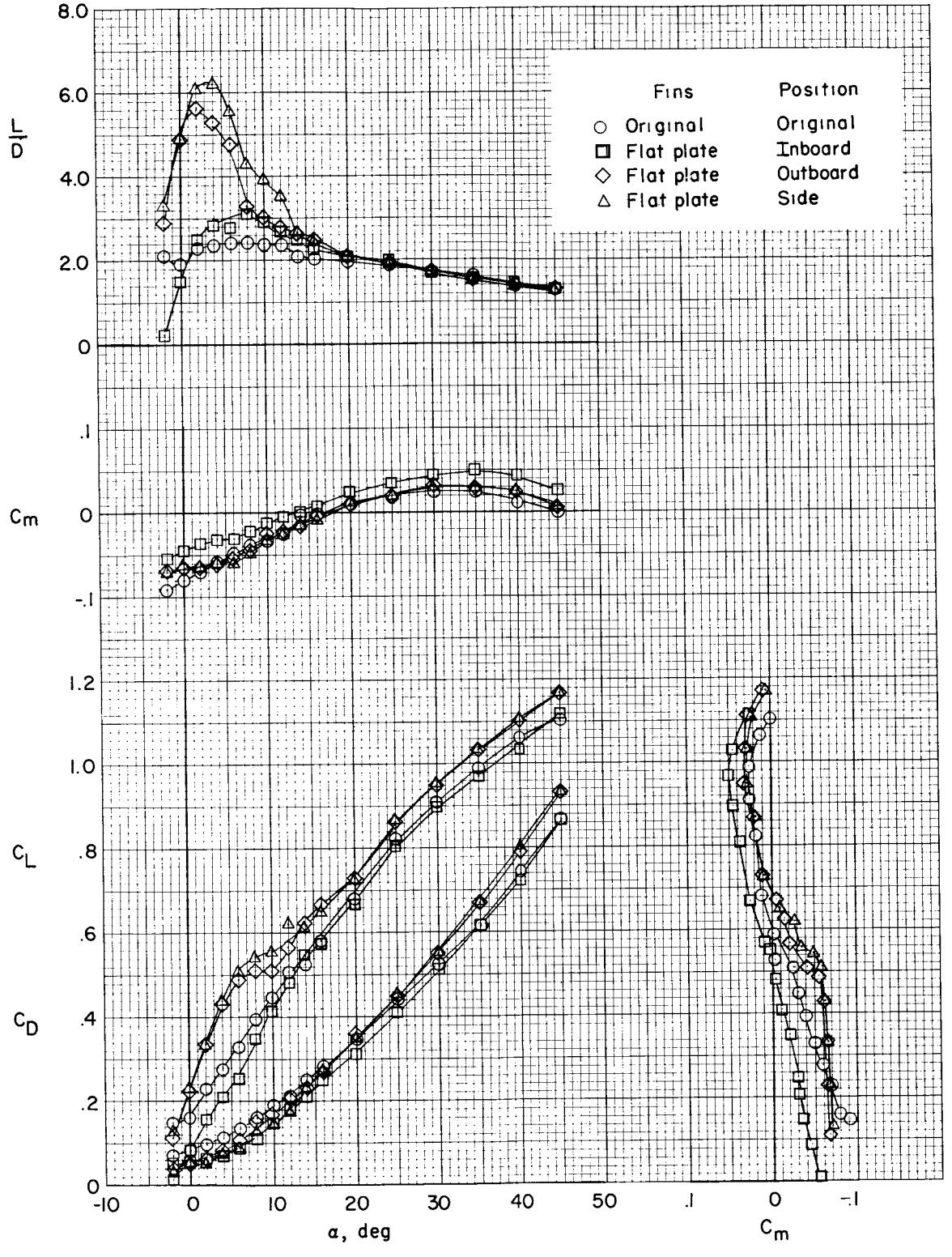

Figure 6.- Effect of fin position on longitudinal stability characteristics of configuration 1. $\beta = 0^{\circ}$; $\Gamma = 45^{\circ}$.

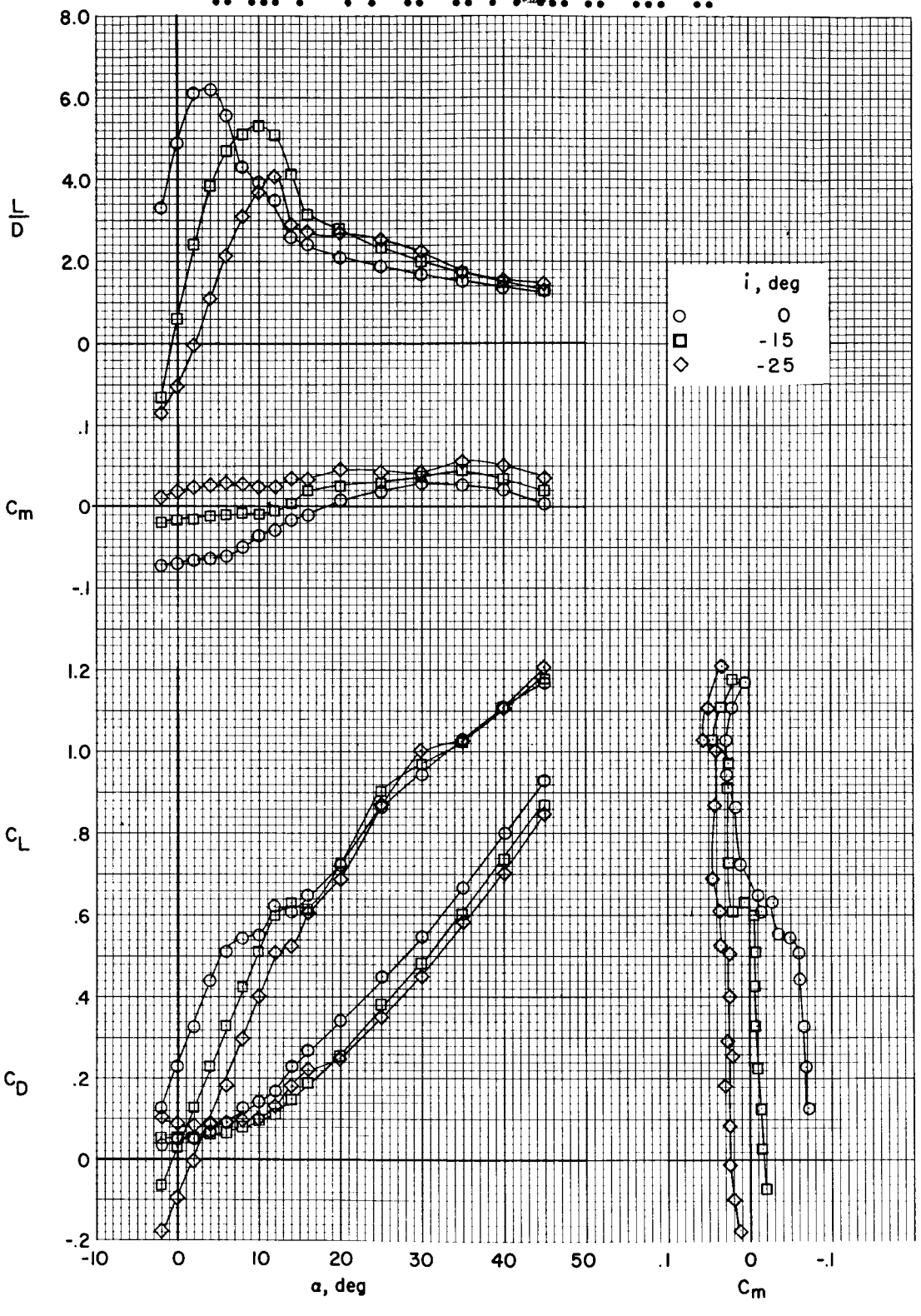

Figure 7.- Effect of flat-plate fin incidence on longitudinal stability characteristics of configuration 1. $\beta = 0^{\circ}$; $\Gamma = 45^{\circ}$.

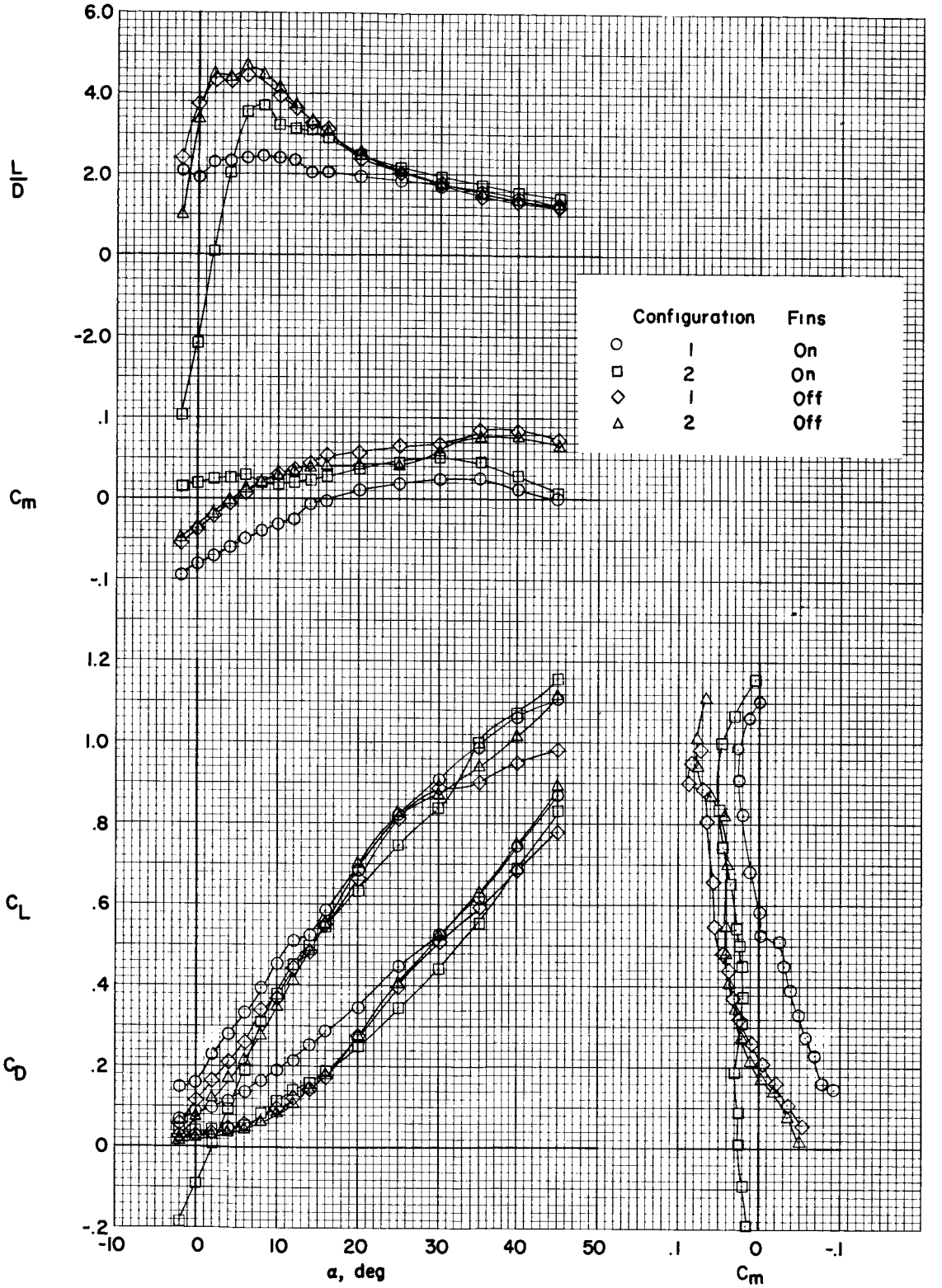

Figure 8.- Longitudinal stability characteristics of configuration 2. $\beta = 0^{\circ}$; $\Gamma = 45^{\circ}$.

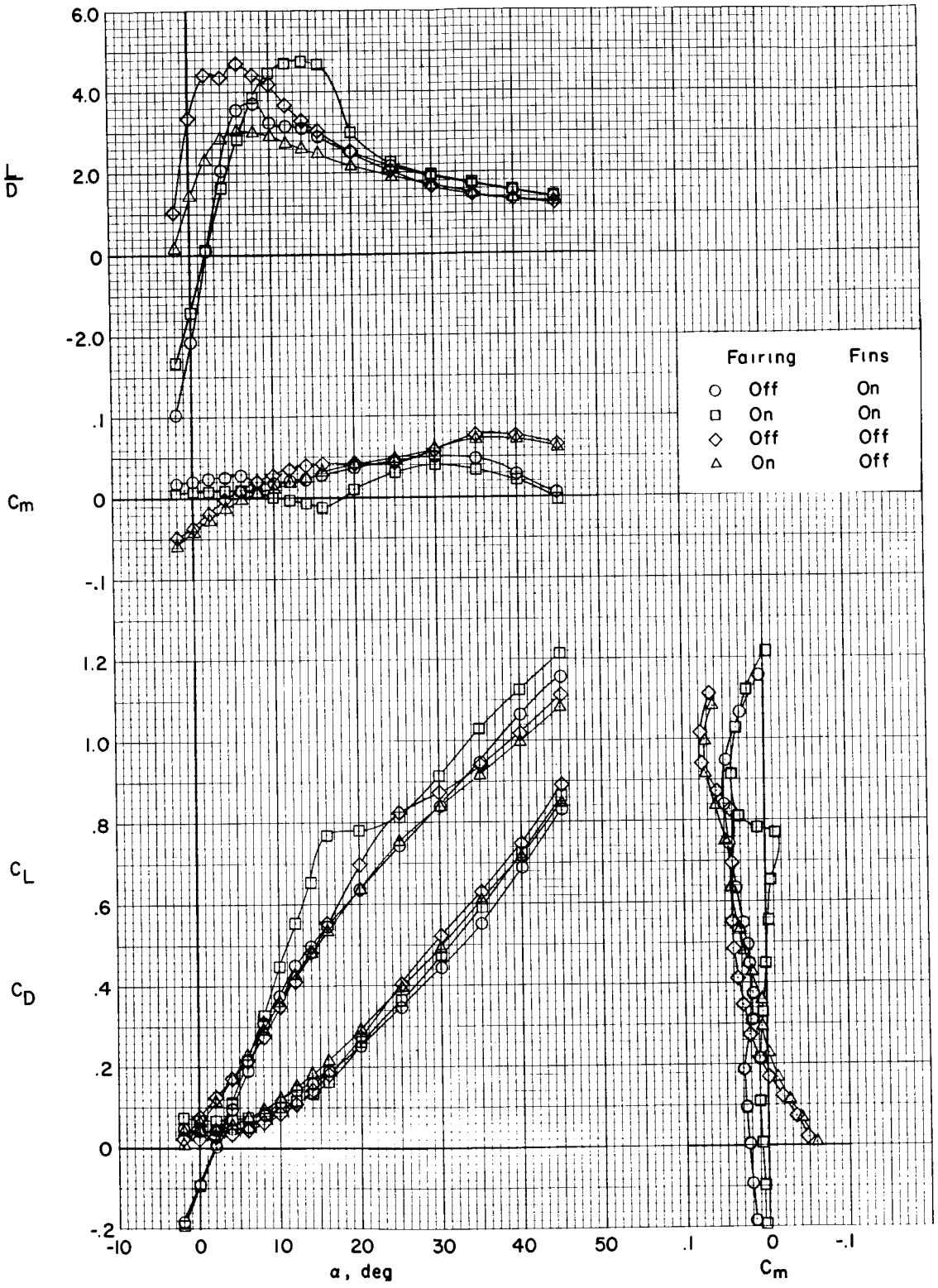

Figure 9.- Effect of fin pylon-body fairing on longitudinal stability characteristics of configuration 2. $\beta = 0^{\circ}$; $\Gamma = 45^{\circ}$.

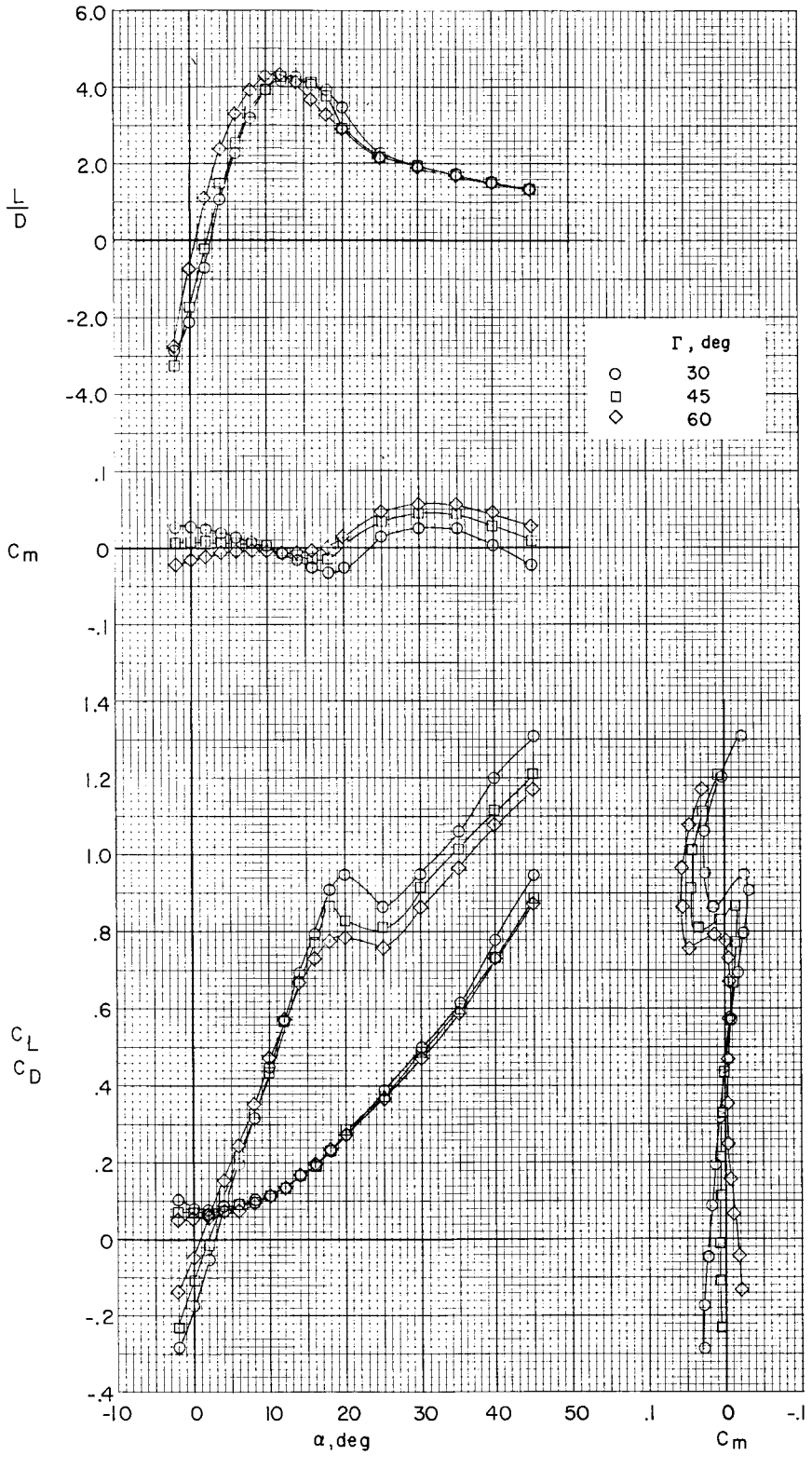

Figure 10.- Effect of fin dihedral angle on the longitudinal stability characteristics of configuration 2. Fairing on; $\beta = 0^{o}$.

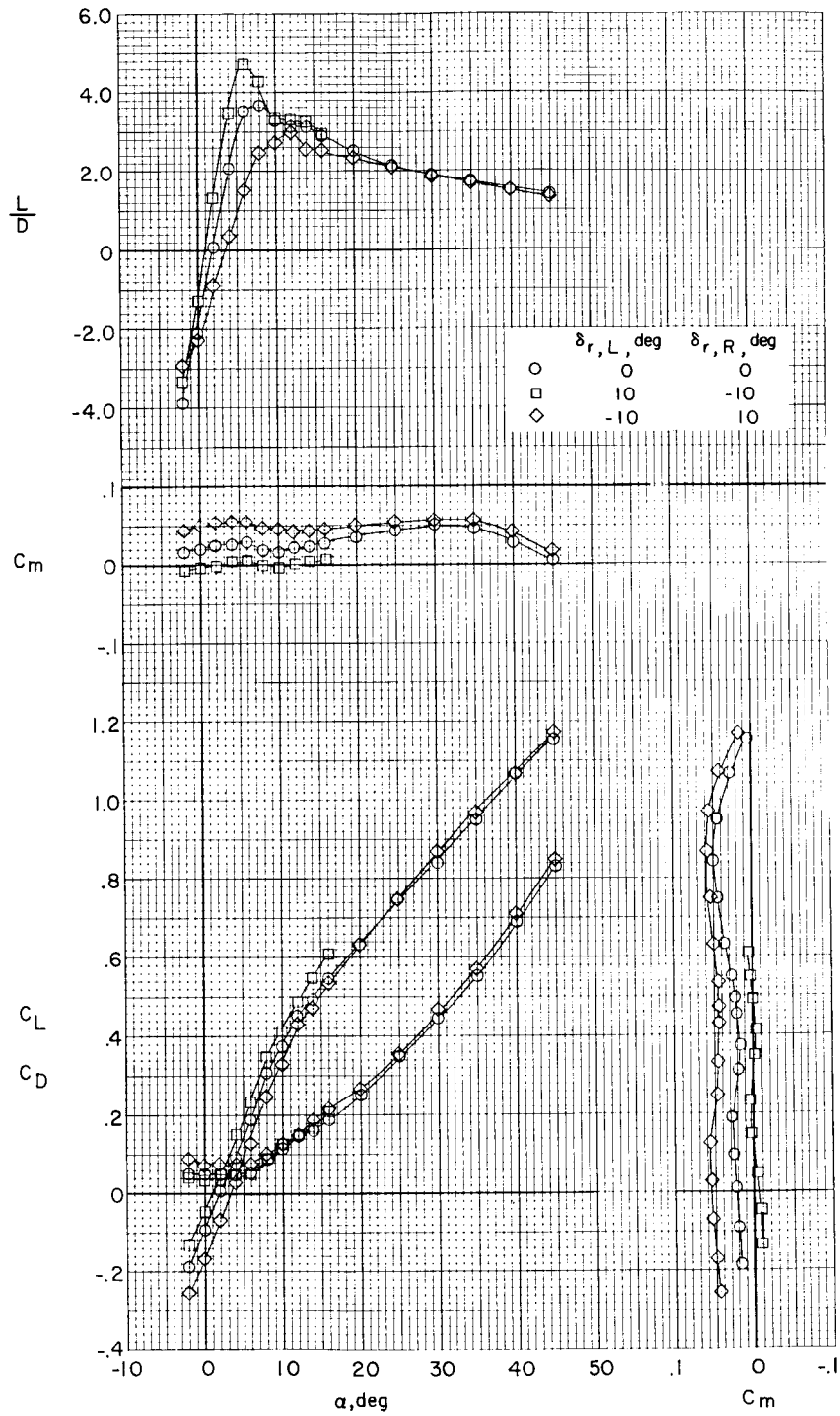

(a) Fairing off.

Figure 11.- Effect of ruddervon deflection as a pitch control on the longitudinal characteristics of configuration 2. $\beta = 0^{\circ}$; $\Gamma = 45^{\circ}$.

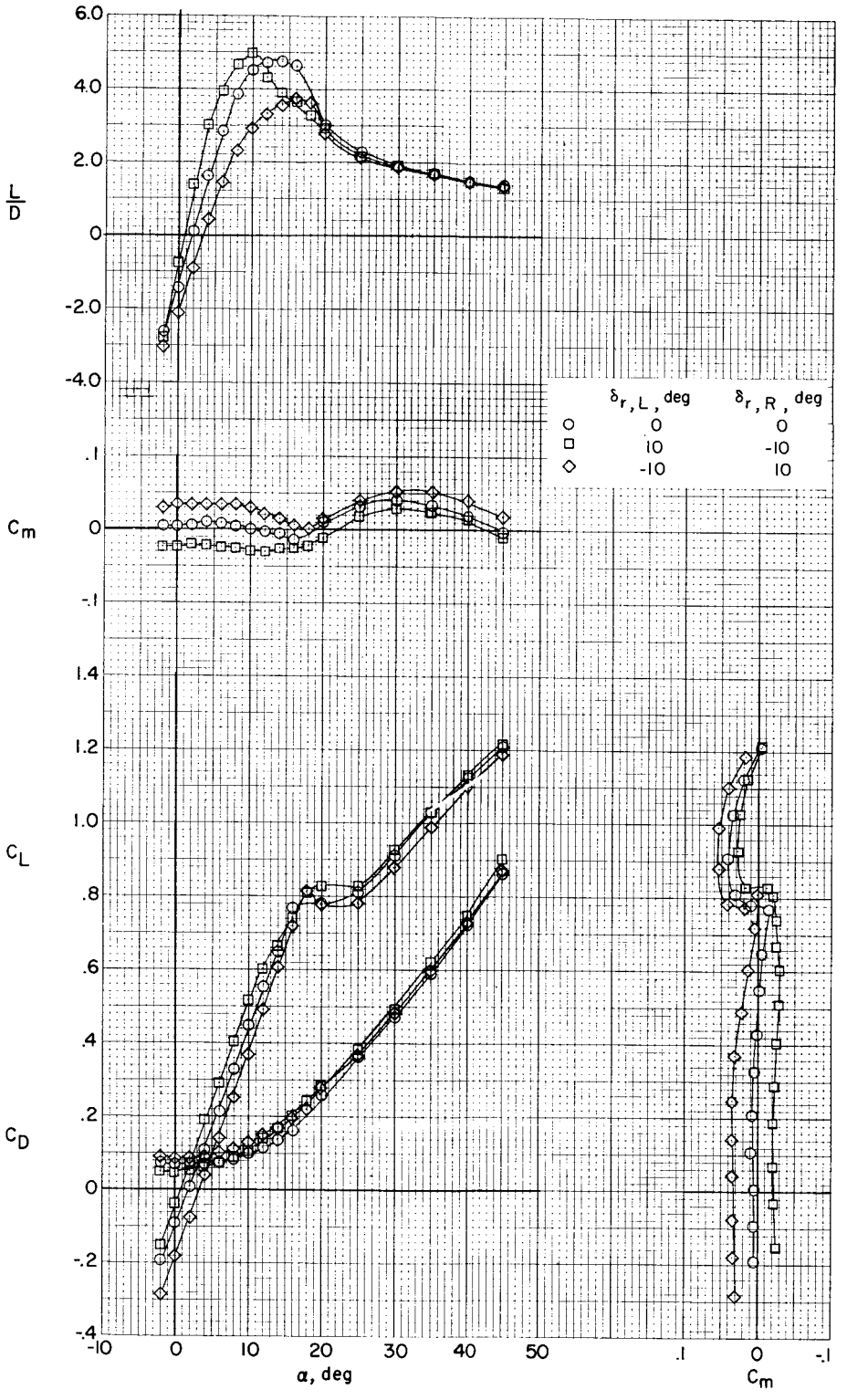

(b) Fairing on.

Figure 11.- Concluded.

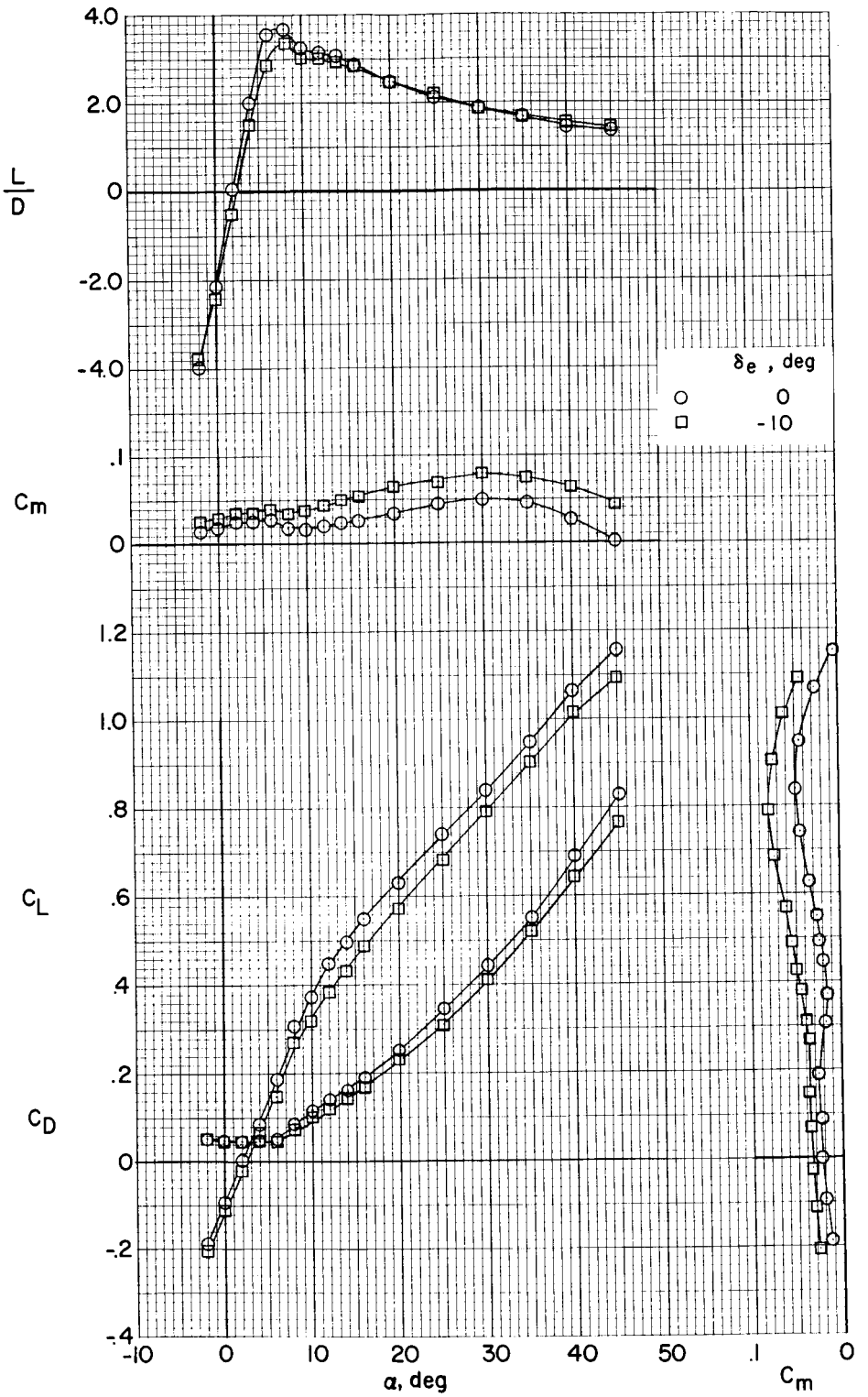

Figure 12.- Effect of elevon deflection as a pitch control on the longitudinal characteristics of configuration 2. Fairing off; $\beta = 0^{\circ}$; $\Gamma = 45^{\circ}$.

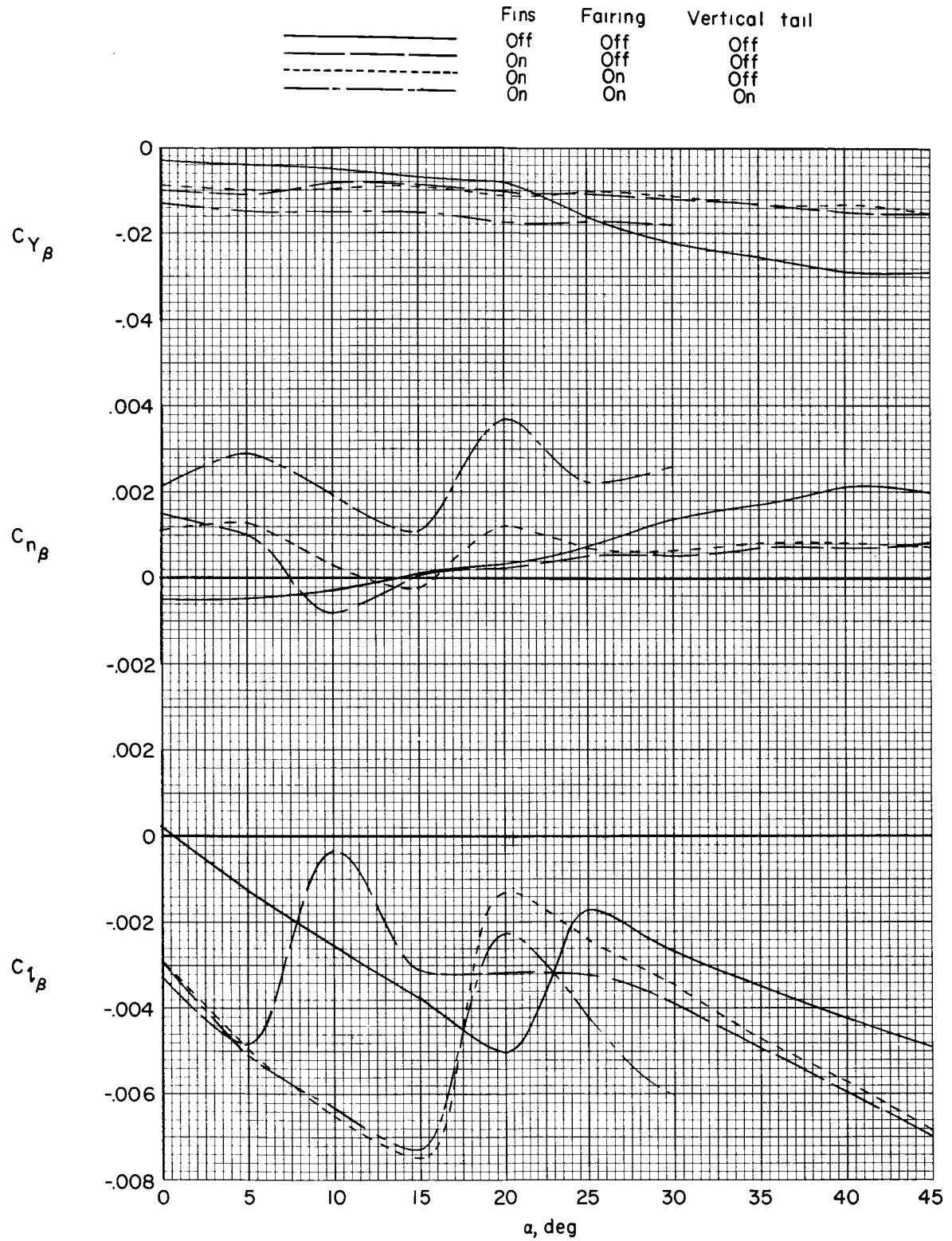

Figure 13.- Lateral stability characteristics of configuration 2. $\Gamma = 45^\circ$.

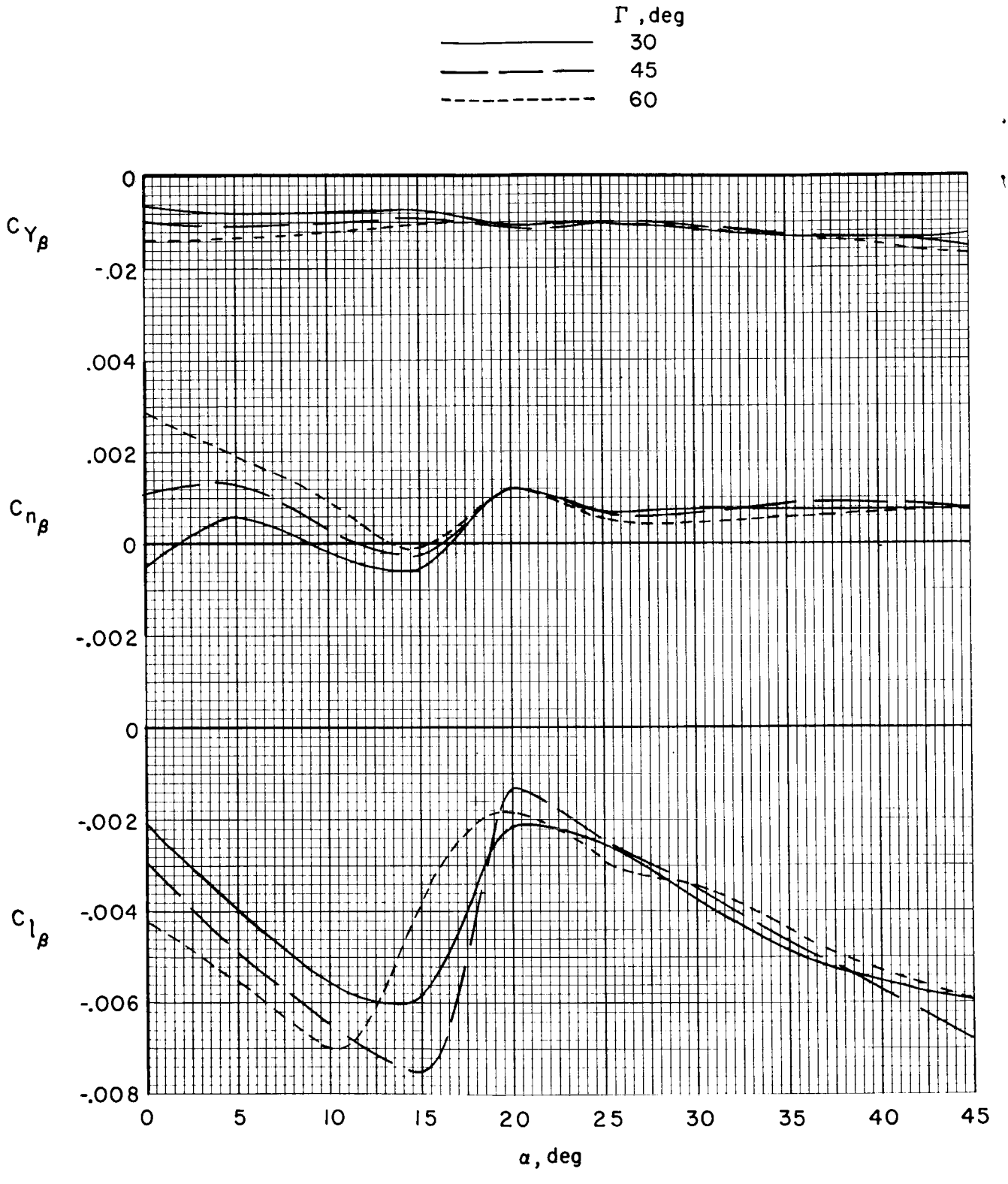

Figure 14.- Effect of fin dihedral angle on the lateral stability characteristics of configuration 2. Fairing on.

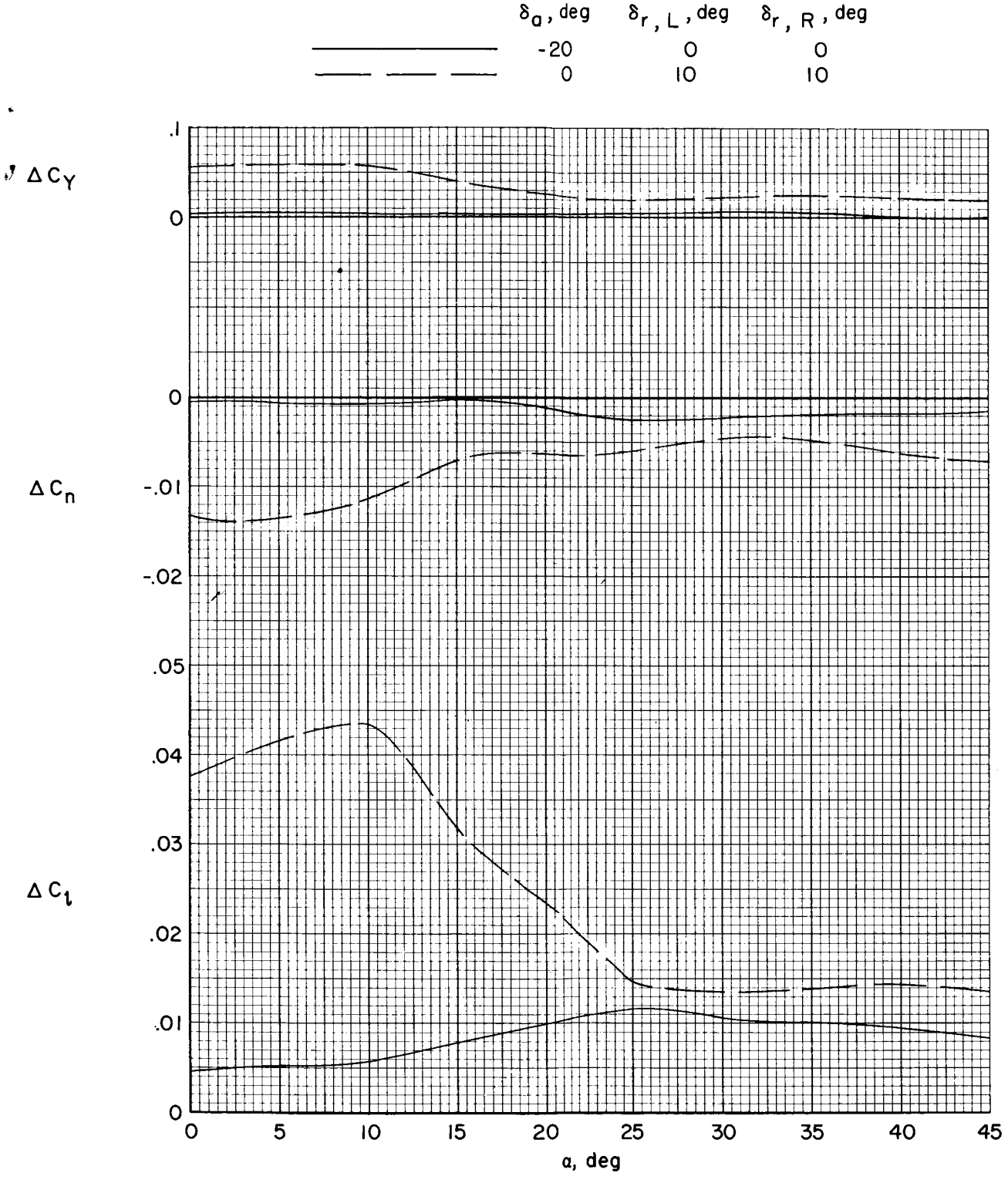

Figure 15.- Effect of aileron and ruddervon deflection on the lateral stability characteristics of configuration 2. Fairing on; $\Gamma = 45^\circ$.